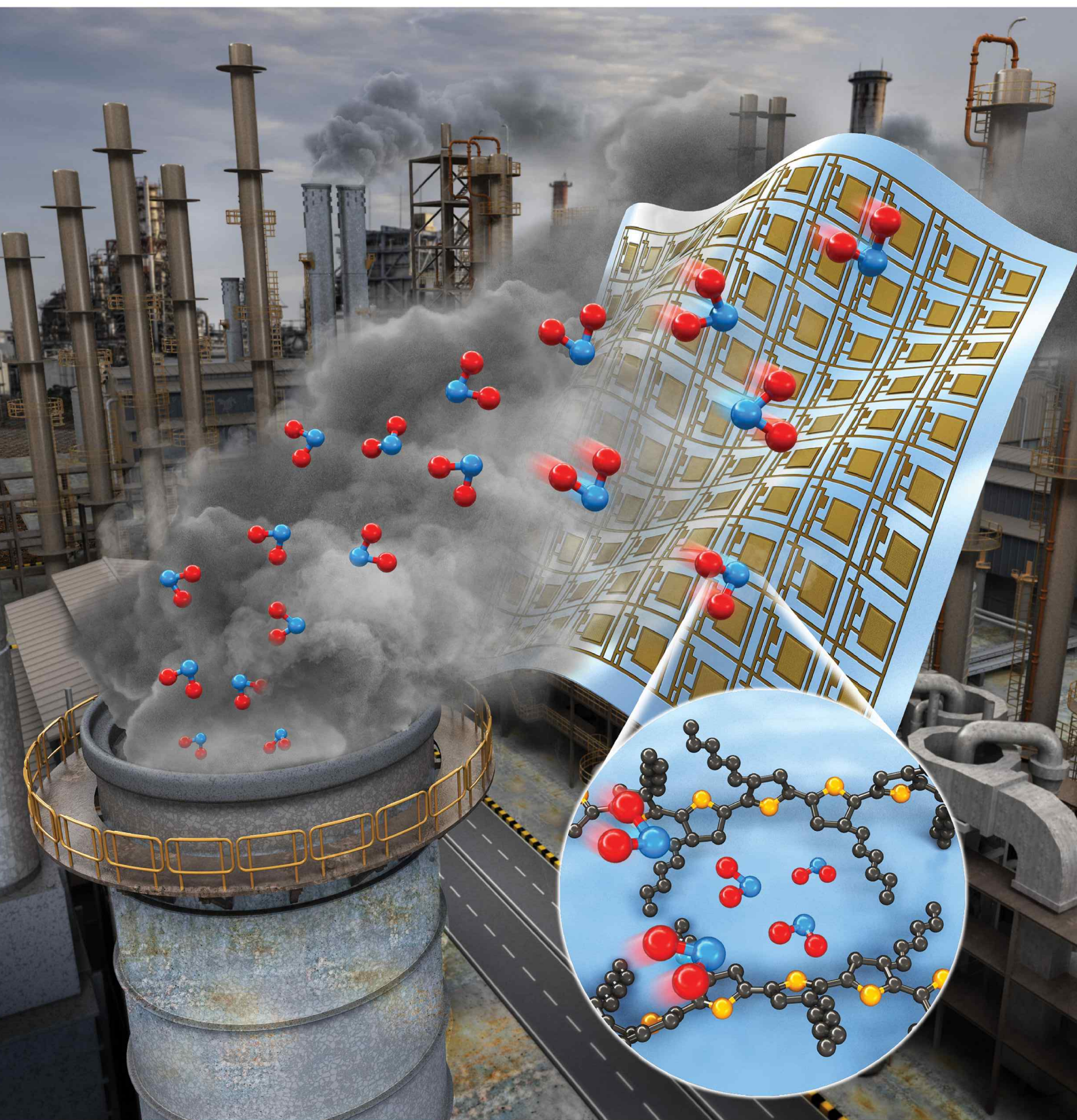


ACS APPLIED MATERIALS & INTERFACES

Xxxxx XX, XXXX
Volume XX
Number XX
pubs.acs.org/acsami



ACS Publications
Most Trusted. Most Cited. Most Read.

www.acs.org

Low-Regioregularity Polythiophene for a Highly Sensitive and Stretchable Gas Sensor

Duho Jang,[§] So Young Park,[§] Hwa Sung Lee,^{*} and Yeong Don Park^{*}Cite This: *ACS Appl. Mater. Interfaces* 2023, 15, 32629–32636

Read Online

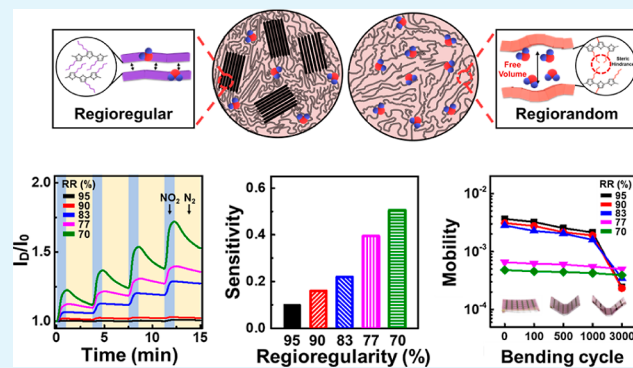
ACCESS |

Metrics & More

Article Recommendations

ABSTRACT: In this study, we examined how the regioregularity of poly(3-hexylthiophene) (P3HT) affects molecular packing, free volume, charge transport, and gas sensing properties. Our results showed that the presence of regular alkyl side chains on the polymer backbone promoted a high degree of structural order in regioregular P3HT molecules, leading to a compact packing density and reduced free volume. Consequently, it was more challenging for NO₂ molecules to interact with the hole charge carriers in the conductive channel. On the other hand, the regiorandom P3HT films displayed a larger free volume, attributed to the irregular side chains, which facilitated the gas–analyte interaction while impeding efficient charge transport. Thus, these films exhibited greater sensitivity to analyte gas molecules. The molecular order, packing density, and hardness of P3HT films were confirmed through the use of multiple techniques, including UV–vis spectroscopy, atomic force microscopy, and grazing-incidence X-ray diffraction. Additionally, the regiorandom P3HT films showed enhanced mechanical flexibility compared to the regioregular films. In conclusion, our findings emphasize that the regularity of polymer molecules plays a significant role in determining the charge carrier transport and gas adsorption characteristics.

KEYWORDS: gas sensor, regioregularity, P3HT, OTFT, NO₂, free volume



1. INTRODUCTION

Conjugated polymers have many advantageous properties that make them suitable for use as active layers in optoelectronics; in particular, they can be fabricated at low cost in solution via a simple process.^{1–5} Their good processing properties in solution are the result of the presence of side chains on the polymer backbone and facilitate the fabrication of affordable large-area devices on plastic substrates.^{6–9} The side chains of the conjugated polymer also strongly influence the molecular order and device performance.^{10–16} Asymmetrically arranged alkyl substituents attached to the polymer backbone give rise to two different regioregularities: head-to-tail (HT) and head-to-head (HH).^{17–19} The regioregularities of polymers are important in that they affect various physical properties of the polymer, such as solubility, modulus, viscoelasticity, thermal behavior, and molecular order. Regioregular side chains enable the molecules to engage in strong van der Waals interactions, which facilitate crystallization.^{20–23} Therefore, the solution becomes more viscous as the regioregularity increases, and the viscosity of the solution increases with the film thickness.^{24–27} In particular, as the regioregularity of the polymer molecule increases, the free volume in the polymer decreases, resulting in poor mechanical properties.^{28–31} A few studies have examined the effects of the positions of alkyl side chains on

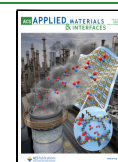
the molecular order in polymer films; however, the influence of regioregularities on the free volume and the resulting gas adsorption properties remains the subject of extensive discussion.

The molecular order governs not only the mechanical properties but also the electrical characteristics of the conjugated polymer films.^{32–34} A previous study reported that regiorandom conjugated polymers limit charge carrier transport owing to the defect-induced charge trap sites resulting from the amorphous regions.^{35,36} Conjugated polymers with regioregular side chains support efficient charge transport; therefore, the regioregularity and molecular order tend to be closely related. Many studies have focused on the high performance of transistors with high regioregularity; however, to the best of our knowledge, the effects of regioregularity on the performance of gas sensor applications have not been widely explored.

Received: April 13, 2023

Accepted: June 7, 2023

Published: June 21, 2023



Highly crystalline polymer films are particularly beneficial for organic transistors because of their π – π interaction; however, a crystalline polymer layer acts as a barrier, making it difficult for gas molecules to penetrate the active layer.^{37–40} The regiorandom-induced free volume in the polymer active layer facilitates exposure of the target gas to the charge carriers in the channel region and promotes interactions between the charge carriers and analyte gas, which enhances the sensitivity and response rates of the sensor.⁴¹ In this study, we systematically investigated the effects of the regioregularity of a conjugated polymer on the molecular order and electrical/sensing characteristics. Notably, regioregularity induced significantly different film morphologies, which resulted in differences in the mechanical properties as well as the transistor and gas-sensing performance. Our study provides useful information and insights into the design of polymeric sensor devices.

2. EXPERIMENTAL DETAILS

2.1. Fabrication of Organic Thin-Film Transistor-Type Gas Sensors Based on a Poly(3-hexylthiophene) Film with Regioregularity. A highly n-doped Si wafer with a 3000 Å thick SiO₂ layer was used as the gate electrode and dielectric. Then, the substrates were prepared for modification with hexamethyldisilazane (HMDS) using sequential sonication in acetone and ethanol for 30 min, respectively, whereupon the substrates were spin-coated with HMDS at 2500 rpm for 30 s and then baked at 125 °C in an oven. Regioregular P3HT (MW = 58 kDa, regioregularity = 95%, PDI = 2.1) and regiorandom P3HT (MW = 38 kDa, regioregularity = 58%, PDI = 2.2) were purchased (Rieke Metals). Blended solutions were prepared by mixing regioregular P3HT and regiorandom P3HT in ratios of 10:0, 9:1, 7:3, 5:5, 3:7, and 0:10 using dichlorobenzene (DCB) as the main solvent. The solution was homogenized by stirring the blend at 50 °C and 800 rpm for 1 h and then allowing it to cool to room temperature. Each blended solution of regiorandom/regioregular P3HT was then spin-cast onto the HMDS-modified SiO₂/Si substrates at 1500 rpm for 60 s. The same method was used to deposit a thin film on a transparent glass substrate for UV–vis spectral analysis. The source and drain electrodes were fabricated by depositing Au through a shadow mask with a channel width of 2000 μ m and a length of 100 μ m on the P3HT thin film by thermal evaporation. The sensor devices were fabricated by wiring the source and drain electrodes onto the sensor platform using silver paste and silver wire.

To conduct the stretching test, Ecoflex substrates were prepared by mixing pre-polymers with their corresponding curing agents in weight ratios of 9:1 and 1:1, respectively. Afterwards, the P3HT-coated SiO₂ substrate was immersed in a hydrofluoric acid solution to remove the polymer film, which was then transferred onto an Ecoflex substrate via a transfer process. For the bending test, a poly(ethylene terephthalate) (PET) film was prepared as the substrate and cleaned in acetone and deionized water, after which a 100 nm thick Al layer was deposited on the PET substrate as the gate electrode by thermal evaporation. Subsequently, a 600 nm thick parylene layer was deposited as the gate dielectric layer via chemical vapor deposition. Finally, the 70 nm thick Au source and drain electrodes were deposited on the P3HT film, as described above. To test the mechanical stability of all the organic thin-film transistors (OTFTs), we performed 100, 500, 1000, and 3000 bending cycles at a fixed bending radius of $r = 5$ mm, followed by the measurement of the electrical characteristics to assess the effect of repeated bending.

2.2. Characterization. The regioregularity of the P3HT was qualitatively and quantitatively determined using ¹H nuclear magnetic resonance (NMR) spectroscopy. The samples were prepared for NMR analysis by dissolving P3HT (0.1 wt %) in deuterated chloroform (CDCl₃). ¹H NMR analyses were conducted on a 400 MHz NMR spectrometer (NMR, Agilent 400-MR, Agilent) operating at standard temperature and pressure. Absorption spectra were

acquired using UV–vis spectroscopy (Lambda 365, PerkinElmer). Grazing-incidence X-ray diffraction (GIXD) patterns were recorded using a high-resolution X-ray diffractometer (SmartLab, Rigaku) to characterize the crystalline structures of the samples. The surface profiles and morphologies of the P3HT thin films were observed by atomic force microscopy (AFM; Multimode 8, Bruker) and optical microscopy (OM; BX51, Olympus). The electrical properties of the P3HT films were characterized under vacuum and at room temperature using a semiconductor analyzer (Keithley 4200-SCS). The gas-sensing performance of the P3HT thin films was characterized using a gas sensor (GASENTEST, Precision Sensor System Inc.) and recorded with a semiconductor analyzer (Keithley 2636 B) at a gate voltage (V_G) of –10 V and drain voltage (V_D) of –10 V to determine the effect of the regioregularity. Sensing tests using NO₂, SO₂, and CO₂ at concentrations from 0 to 100 ppm were carried out under low-moisture ambient conditions by maintaining the total flow rate at 500 sccm [relative humidity (RH) = 14.5%]. Bending tests were conducted using a bending machine (BM-100, ECOPIA) under ambient conditions.

3. RESULTS AND DISCUSSION

P3HT regioregularity refers to the portion of P3HT with HT coupling within the polymer chain.⁴² Figure 1 shows the three

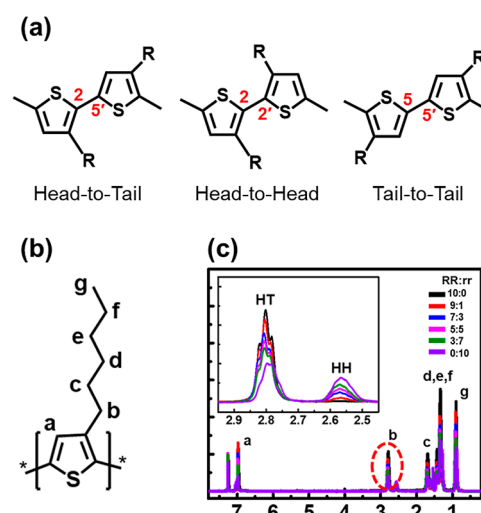


Figure 1. (a) Molecular structures of P3HT with three different types of couplings: HT, HH, and TT. (b) Schematic structure of a single unit of P3HT with proton labeling. (c) ¹H NMR spectra of the P3HT blends with different regioregular–regiorandom P3HT ratios. The inset shows the region of interest for the calculation of the regioregularity of the P3HT.

Table 1. Average Regioregularity Values of P3HT with the Regioregular–Regiorandom P3HT Ratios

RR/rr	HT	HH	regioregularity (%)
10:0	1.00	0.05	95
9:1	1.00	0.08	90
7:3	1.00	0.21	83
5:5	1.00	0.30	77
3:7	1.00	0.42	70
0:10	1.00	0.73	58

different couplings of P3HT: HT, HH, and tail-to-tail (TT). Regioregular P3HT, characterized by a high proportion of HT–HT couplings, is stable, planar, and highly crystalline. In contrast, regiorandom P3HT has a high proportion of non-regional couplings, such as HT–TT, HT–HH, and TT–HH,

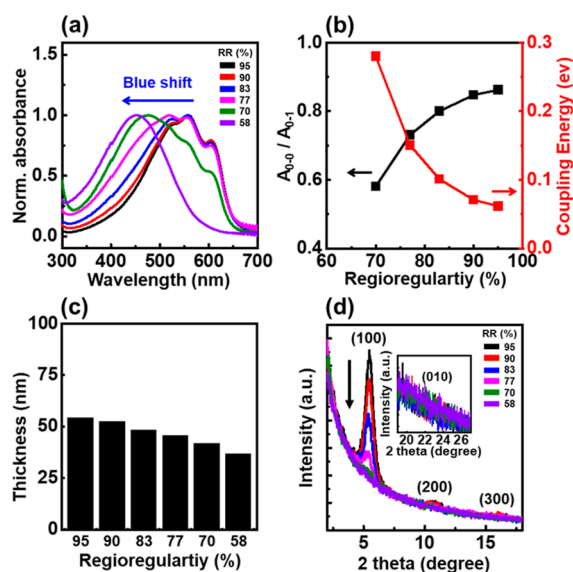


Figure 2. (a) Normalized UV-vis spectra of P3HT thin films depending on the regioregularity. (b) Plot of the A_{0-0}/A_{0-1} ratio (left axis) and interchain coupling energy (W) information (right axis). (c) Bar chart of the P3HT thin film thickness vs regioregularity. (d) GIXD patterns (linear scale) of spin-cast P3HT thin films with the addition of regiorandom P3HT. The downward arrow indicates the direction of decreasing regioregularity.

resulting in an amorphous structure. The regioregularity of the P3HT blends with different regioregular–regiorandom P3HT ratios was investigated by analyzing the ^1H NMR signals at 2.80 and 2.58 ppm, attributable to HT and HH couplings, respectively. The regioregularity of P3HT was quantitatively estimated by integrating the areas of these two peaks of the α -methylene-H on the ^1H NMR spectrum. Thus, the degree of regioregularity can be calculated as the ratio of the integrated area of the peak at 2.80 to that at 2.58 ppm. Using this approach, the regioregular P3HT used in this study was estimated to have $\sim 95\%$ regioregularity, whereas the

regiorandom P3HT had $\sim 58\%$ regioregularity. The average regioregularity of P3HT was varied by changing the blend ratio by mixing P3HT with regioregular and regiorandom regions in various ratios (Table 1).

UV-vis spectra were recorded to investigate the variation in the molecular order and thickness of the P3HT blend films with the regioregularity (Figure 2a). First, for 95% regioregular P3HT, the $A_{(0-2)}$ peak, representing the intrachain π – π^* transition, was observed at ~ 520 nm. Furthermore, the $A_{(0-1)}$ and $A_{(0-0)}$ peaks, indicating P3HT interchain transitions, were observed at ~ 559 and ~ 606 nm, respectively.⁴³ However, as the regioregularity of P3HT decreased, the intensities of the $A_{(0-1)}$ and $A_{(0-0)}$ peaks decreased, and the $A_{(0-2)}$ peak was blue-shifted relative to that of the regioregular P3HT thin film. This was caused by the high steric hindrance of the irregular side chains.⁴⁴ When the ratio of RR/rr P3HT was increased to 7:3, the characteristics of crystalline P3HT thin films were still exhibited. However, the higher the proportion of regiorandom P3HT, the weaker the π – π stacking between regioregular P3HT chains because of the stronger steric hindrance. The UV-vis absorption spectra were indicative of the existence of H-aggregates with weak coupling bonds between the P3HT chains, which quantitatively represent the changes in the crystallinity of the P3HT thin films. The intensity of the $A_{(0-0)}$ peak is reduced by increasing exciton coupling, and the value of the interchain coupling energy W can be calculated using the following equation

$$\frac{A_{0-0}}{A_{0-1}} \approx \frac{n_{0-1}}{n_{0-0}} \left(\frac{1 - 0.24W/E_p}{1 + 0.073W/E_p} \right)^2 \quad (1)$$

where E_p is the symmetrical vinyl stretching vibration energy ($E_p = 0.18$ eV), and n is the refractive index ($n_{0-1}/n_{0-0} = 0.97$).⁴⁵ The increase in the conjugation length of P3HT can be demonstrated by the increase in $A_{(0-0)}/A_{(0-1)}$ because the P3HT thin film with high regioregularity has a low W value. Therefore, we compared the $A_{(0-0)}/A_{(0-1)}$ values of each P3HT thin film to measure the effect of the change in the

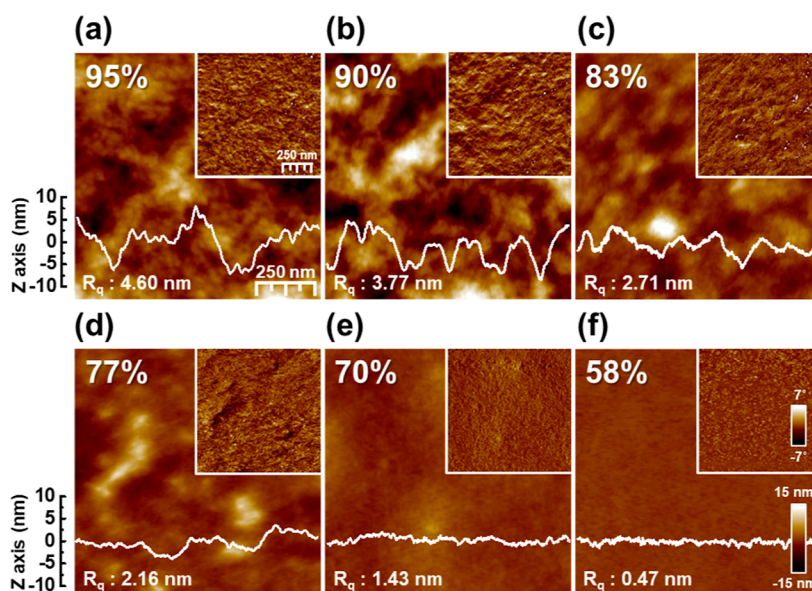


Figure 3. AFM phase and height images ($1 \times 1 \mu\text{m}$) of the surface of the P3HT thin films with (a) 95, (b) 90, (c) 83, (d) 77, (e) 70, and (f) 58% regioregularity.

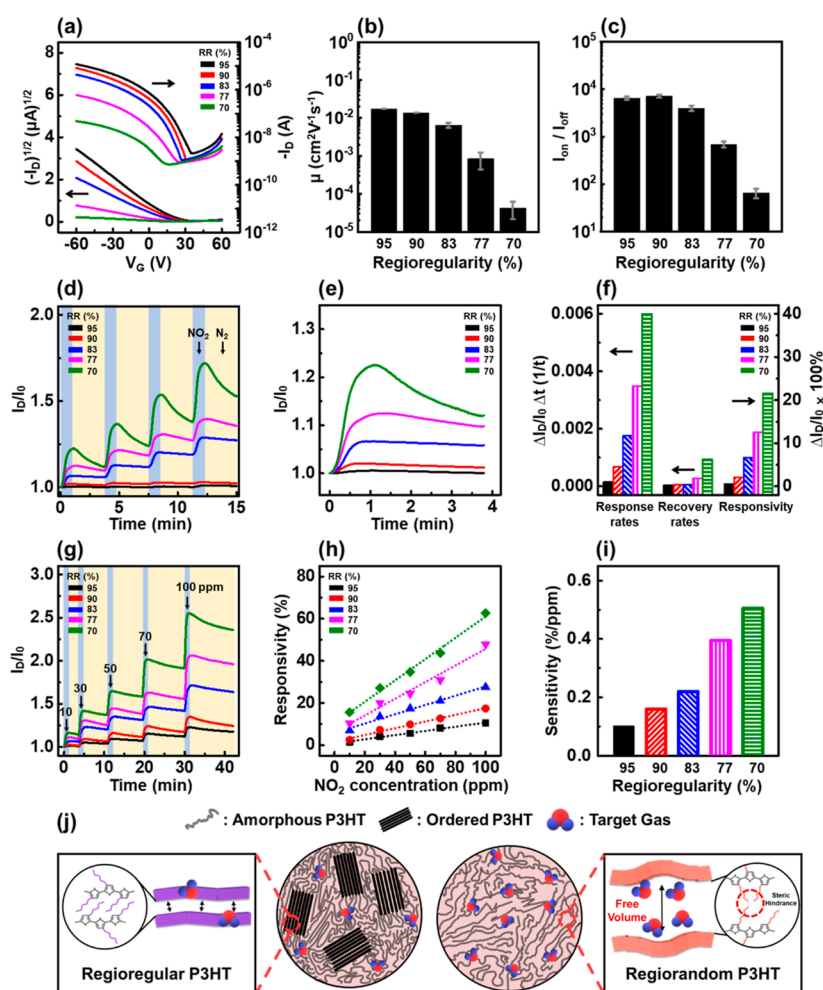


Figure 4. (a) Transfer characteristics (I_D vs V_G at $V_D = -60$ V) of the P3HT thin film with the regioregularity. (b,c) Calculated field-effect mobilities and the on/off ratio changes of P3HT thin films with regioregularity. (d) Repeated gas-sensing curve for gas sensors based on P3HT thin films; (e) magnifications of the first stages of the curves in (d); (f) summary of gas sensing parameters. (g) Dependence of the dynamic gas-sensing performance of the P3HT thin film on the regioregularity. (h) Calculated responsivity of the P3HT thin films plotted as a function of the NO_2 concentration and (i) sensitivity vs regioregularity calculated from the slopes of the plots in (h). (j) Schematic of gas adsorption of P3HT films with regioregularity.

regioregularity on the crystallinity of the P3HT thin films (Figure 2b). As the regioregularity of P3HT decreased, the molecular order of the thin film decreased, and the thickness also tended to decrease because of the low viscosity of the solution (Figure 2c).

The GIXD analysis along the out-of-plane direction confirmed the change in the crystalline structure of the P3HT thin film with the regioregularity of the P3HT (Figure 2d). For the P3HT thin film with 95% regioregularity, an intense (100) diffraction peak was observed at $\sim 5.4^\circ$, which represents the interchain distance in the P3HT lamellae.⁴⁶ In addition, low-intensity (200) and (300) peaks were observed at 11 and 15.7° , respectively. As the regioregularity of P3HT decreased, the intensity of the (100) diffraction peak in the out-of-plane direction gradually decreased. These results corresponded well with the change in molecular order in the P3HT thin films calculated from the UV–vis absorption data. In addition, the (010) diffraction peaks, which represent the π – π stacking of P3HT chains, were not observed in all samples regardless of the regioregularity, and this indicates that each of the films had an edge-on structure.

The changes in the surface profile and nanoscale morphology with the regioregularity of P3HT were studied using AFM (Figure 3). The height and phase images of the 95% regioregular P3HT thin film revealed considerable roughness and high rigidity, respectively. However, the roughness and hardness of the thin film started to decrease with decreasing regioregularity, and the regiorandom P3HT thin film exhibited a smooth surface morphology and soft characteristics. The decrease in both rigidity and roughness indicated that the crystallinity of the regioregular P3HT had degraded and that the thin film had become amorphous owing to the steric hindrance of the irregular side chain.^{36,47} These results indicate that the P3HT film exhibits flexible characteristics as the regioregularity of P3HT decreases.

To investigate the charge transport characteristics with respect to the regioregularity of P3HT, the transfer curve of each P3HT thin film was examined with a bottom-gate, top-contact transistor geometry. As the regioregularity of P3HT decreased, the drain-current levels of the charge transfer curves gradually decreased (Figure 4a);³⁶ accordingly, the field effect mobility values decreased dramatically from 1.7×10^{-2} to $4.2 \times 10^{-5} \text{ cm}^2 \text{ V}^{-1} \text{ s}^{-1}$, and the on/off ratio also decreased from 6

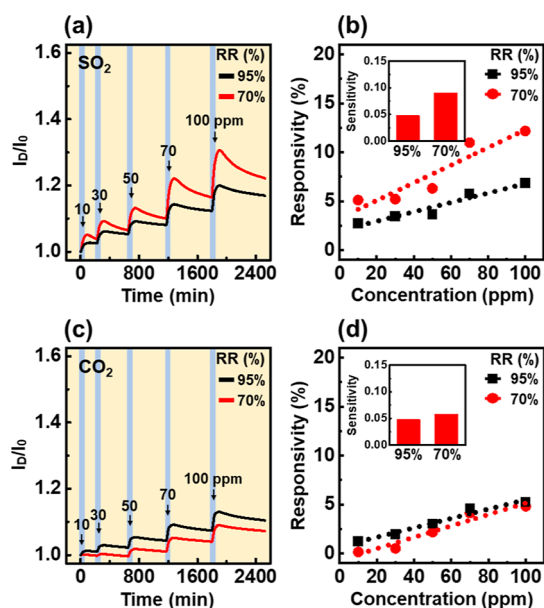


Figure 5. Dependence of the dynamic gas-sensing performance of the P3HT thin film on the regioregularity: dynamic response curve of the P3HT thin films for (a) SO₂ and (c) CO₂. Calculated responsivity curve and sensitivity (inset) for (b) SO₂ and (d) CO₂.

$\times 10^3$ to 6×10 (Figure 4b,c). In addition, regiorandom P3HT (58%) had a very low drain current; therefore, the charge-transfer characteristics could not be measured. We confirmed that the molecular order decreased as the regioregularity of the P3HT ratio decreased; thus, the charge transport performance was also expected to decrease because of the defects caused by the irregular chain configuration.

The NO₂ gas-sensing parameters of the P3HT thin film with regioregularity were repeatedly measured (Figure 4d–i). In these experiments, the P3HT thin films with regioregularity were repeatedly exposed to 10 ppm NO₂ gas for 20 s and purged with air for 200 s. The source-drain current was measured at a low current level, -10 V gate voltage (V_G), and -10 V drain voltage (V_D). The drain current of all P3HT films increased dramatically owing to the p-doping effect of NO₂ upon injection of the gas, regardless of the regioregularity (Figure 4d).^{48,49} The 70% regioregularity P3HT film exhibited a higher drain current level, which resulted in a superior response rate, recovery rate, and responsivity. These properties were quantified by calculating the values of $\Delta R/\Delta t$, $\Delta R/\Delta t$, and $\Delta I_D/I_0$ obtained from the increasing and decreasing curves of the gas response time–current curves (Figure 4f). The enhanced gas-sensing performance of the regiorandom P3HT thin films might be a result of the increased free volume, referred to as empty spaces or voids, due to the irregular side chain configuration. Regiorandom P3HT thin films have abundant free volume because the steric hindrance affects the packing density and molecular order of the P3HT chains within the film, which in turn influences the charge carrier transport and optical properties. A larger free volume would facilitate gas adsorption, which would enhance the gas-sensing performance. Following the injection of NO₂ gas, the gas molecules must penetrate the channel region that forms a few nanometers above the interface between the active and dielectric layers to enable the NO₂ gas to be detected. In the regiorandom P3HT film, the large free volume allows the NO₂ gas to reach the channel more easily. This explains the superior

sensing performance of the 70% regioregularity P3HT film as a result of the large free volume derived from the irregular chain configuration (Figure 4j).

The variation in the gas-sensing performance with the concentration of NO₂ was investigated by measuring the dynamic sensing properties (Figure 4g). We measured the change in the drain current as the concentration of NO₂ gas was increased from 10 to 100 ppm in increments of 20 ppm. The gas injection time was kept constant at 20 s for each measurement, and the recovery time increased by 100 s as the injected amount increased. The current increased linearly regardless of the regioregularity and confirmed that, similar to previous gas-sensing measurements, the film with 70% regioregularity P3HT delivered the best sensing performance. We calculated the sensitivity to NO₂ gas from the slope of the responsivity as a function of the NO₂ content (Figure 4h,i). As a result, as the regioregularity of P3HT decreased, the gas sensitivity increased, and the evaluated sensitivity of the 70% regioregularity P3HT film was more than five times larger than that of the 95% regioregularity P3HT film.

We additionally measured the sensing performance of the 95 and 70% regioregularity P3HT films with respect to SO₂ and CO₂ under the same conditions (Figure 5a–d). Upon exposure of the gas sensors to various concentrations of SO₂, a strong electron-withdrawing molecule similar to NO₂, the drain current of the devices also increased as a result of p-doping. The sensing performance and sensitivity of the P3HT film with 70% regioregularity were superior to those of the 95% regioregularity P3HT film. A similar tendency was observed during the dynamic sensing of CO₂; however, the sensing response and sensitivity were almost negligible, most likely because the CO₂ molecules are nonpolar and consist of a symmetric dipole.

Previous AFM analyses confirmed that regiorandom P3HT exhibits soft characteristics. This means that organic transistors with low regioregularity have increased flexibility, which is a significant advantage over devices with high regioregularity.⁵⁰ Stretching tests were conducted on each P3HT film at 0, 10, 30, 50, and 100% strain (Figure 6a). The results showed that cracking began to occur at approximately 30% strain for the P3HT film with 95% regioregularity. However, as the regioregularity of P3HT decreases, the strain strength at which cracking begins gradually increases. At a P3HT regioregularity of 77% or less, the P3HT film no longer developed cracks, even with 100% applied strain. This is because the larger amorphous regions of the regiorandom P3HT have the effect of increasing the softness of the film, allowing it to withstand more significant strain while maintaining excellent film flexibility.

We subjected each P3HT film to a bending test using a bending radius of 5 mm in both directions and measured the change in charge-carrier mobility with the number of bending cycles. The results confirmed that the charge carrier mobility of all transistors was generally maintained up to approximately 1000 bending cycles, regardless of the regioregularity of P3HT. However, after 1000 bending cycles, a sharp decrease in charge-carrier mobility was observed for the regioregular P3HT film. In contrast, devices with regiorandom P3HT films maintained their charge-carrier mobility even after approximately 3000 bending cycles. This is because the higher the regiorandom P3HT ratio, the more voids exist, making it less susceptible to external forces. As these voids are not occupied

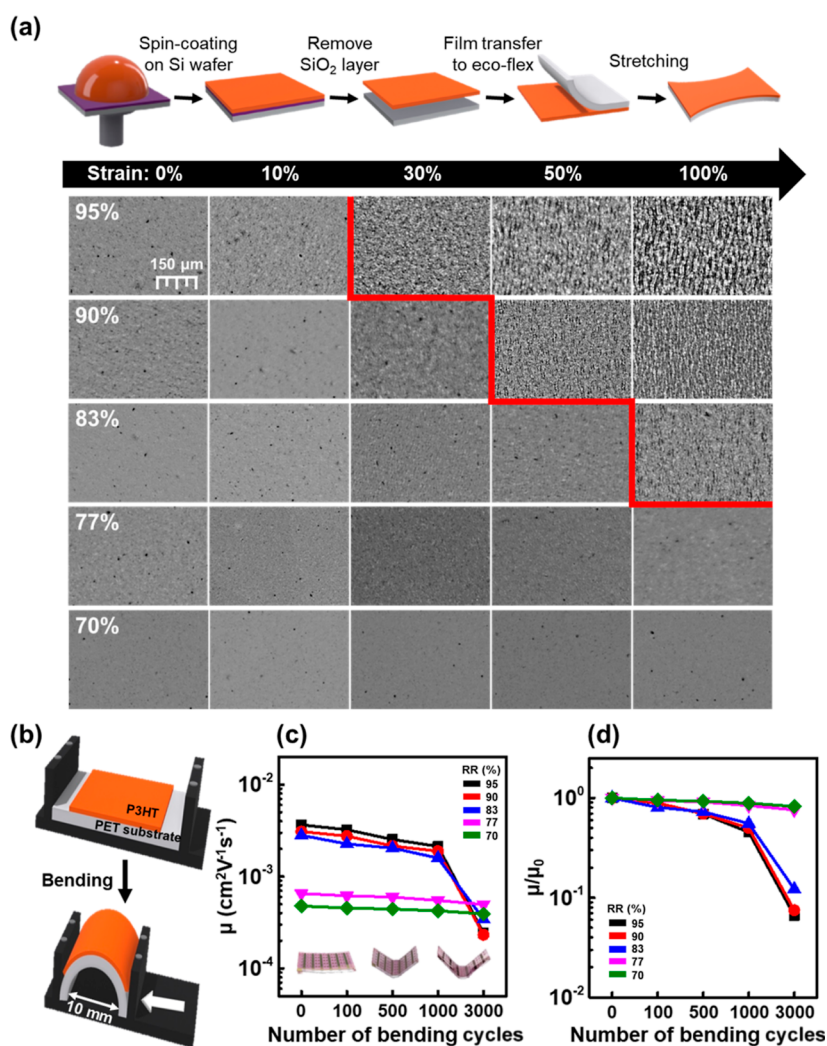


Figure 6. (a) Schematic illustration of the stretching test and OM images of the stretched P3HT thin film with regioregularity. (b) Schematic illustration of the bending machine and bending test. (c) Changes in the charge carrier mobility of the P3HT thin films with the number of bending cycles, and (d) normalized charge carrier mobility.

by atoms or molecules, they are free to move or deform when an external force is applied.

4. CONCLUSIONS

In this study, we investigated the effect of P3HT regioregularity on the molecular packing, free volume, and corresponding changes in charge carrier transport and gas-sensing properties. The structural order of the regioregular P3HT molecules increased significantly because of the presence of regular alkyl side chains on the polymer backbone. The reduced free volume caused by the high packing density made it difficult for NO₂ molecules to interact with the hole charge carriers in the conductive channel. The large free volume induced by the irregular side chains in P3HT interferes with efficient charge transport; however, the free volume simultaneously facilitates gas-analyte interaction. Therefore, the regiorandom P3HT films exhibited enhanced responsivity to analyte gas molecules. The molecular order, packing density, and hardness of the P3HT films were confirmed using UV–vis spectroscopy, AFM, and GIXD. The regiorandom P3HT films also exhibited greater mechanical flexibility. Our findings showed that the regularity of polymer molecules plays an

important role in charge carrier transport and gas adsorption characteristics.

AUTHOR INFORMATION

Corresponding Authors

Hwa Sung Lee – Department of Materials Science and Chemical Engineering, Hanyang University, Ansan 15588, Republic of Korea; orcid.org/0000-0001-9131-810X; Email: hslee78@hanyang.ac.kr

Yeong Don Park – Department of Energy and Chemical Engineering, Incheon National University, Incheon 22012, Republic of Korea; orcid.org/0000-0002-1615-689X; Email: ydpark@inu.ac.kr

Authors

Duho Jang – Department of Energy and Chemical Engineering, Incheon National University, Incheon 22012, Republic of Korea

So Young Park – Department of Energy and Chemical Engineering, Incheon National University, Incheon 22012, Republic of Korea

Complete contact information is available at: <https://pubs.acs.org/10.1021/acsami.3c05278>

Author Contributions

[§]D.J. and S.Y.P. equally contributed to this work.

Notes

The authors declare no competing financial interest.

ACKNOWLEDGMENTS

This work was supported by the National Research Foundation of Korea (NRF) grant funded by the Korea government (MSIT) (no. 2023R1A2C1005218).

REFERENCES

- (1) Zhang, C.; Luo, Y.; Xu, J.; Debligny, M. Room Temperature Conductive Type Metal Oxide Semiconductor Gas Sensors for NO₂ Detection. *Sens. Actuators, A* **2019**, *289*, 118–133.
- (2) Hong, S.; Wu, M.; Hong, Y.; Jeong, Y.; Jung, G.; Shin, W.; Park, J.; Kim, D.; Jang, D.; Lee, J. H. FET-Type Gas Sensors: A Review. *Sens. Actuators, B* **2021**, *330*, 129240.
- (3) Wang, Y.; Zhang, J.; Zhang, S.; Huang, J. OFET Chemical Sensors: Chemical Sensors Based on Ultrathin Organic Field-Effect Transistors. *Polym. Int.* **2021**, *70*, 414–425.
- (4) He, C.; Cheng, J.; Zhang, X.; Douthwaite, M.; Pattison, S.; Hao, Z. Recent Advances in the Catalytic Oxidation of Volatile Organic Compounds: A Review Based on Pollutant Sorts and Sources. *Chem. Rev.* **2019**, *119*, 4471–4568.
- (5) Surya, S. G.; Raval, H. N.; Ahmad, R.; Sonar, P.; Salama, K. N.; Rao, V. R. Organic Field Effect Transistors (OFETs) in Environmental Sensing and Health Monitoring: A Review. *TrAC, Trends Anal. Chem.* **2019**, *111*, 27–36.
- (6) Wang, F.; Dai, Y.; Wang, W.; Lu, H.; Qiu, L.; Ding, Y.; Zhang, G. Incorporation of Heteroatoms in Conjugated Polymers Backbone toward Air-Stable, High-Performance n-Channel Unencapsulated Polymer Transistors. *Chem. Mater.* **2018**, *30*, 5451–5459.
- (7) Peng, B.; Huang, S.; Zhou, Z.; Chan, P. K. L. Solution-Processed Monolayer Organic Crystals for High-Performance Field-Effect Transistors and Ultrasensitive Gas Sensors. *Adv. Funct. Mater.* **2017**, *27*, 1700999.
- (8) Di, C. A.; Shen, H.; Zhang, F.; Zhu, D. Enabling Multifunctional Organic Transistors with Fine-Tuned Charge Transport. *Acc. Chem. Res.* **2019**, *52*, 1113–1124.
- (9) Kang, B.; Lee, W. H.; Cho, K. Recent Advances in Organic Transistor Printing Processes. *ACS Appl. Mater. Interfaces* **2013**, *5*, 2302–2315.
- (10) Elsenbaumer, R. L.; Jen, K. Y.; Oboodi, R. Processible and Environmentally Stable Conducting Polymers. *Synth. Met.* **1986**, *15*, 169–174.
- (11) Luo, N.; Ren, P.; Feng, Y.; Shao, X.; Zhang, H. L.; Liu, Z. Side-Chain Engineering of Conjugated Polymers for High-Performance Organic Field-Effect Transistors. *J. Phys. Chem. Lett.* **2022**, *13*, 1131–1146.
- (12) Moro, S.; Siemons, N.; Drury, O.; Warr, D. A.; Moriarty, T. A.; Perdigão, L. M. A.; Pearce, D.; Moser, M.; Hallani, R. K.; Parker, J.; McCulloch, I.; Frost, J. M.; Nelson, J.; Costantini, G. The Effect of Glycol Side Chains on the Assembly and Microstructure of Conjugated Polymers. *ACS Nano* **2022**, *16*, 21303–21314.
- (13) Yang, J.; Wang, H.; Chen, J.; Huang, J.; Jiang, Y.; Zhang, J.; Shi, L.; Sun, Y.; Wei, Z.; Yu, G.; Guo, Y.; Wang, S.; Liu, Y. Bis-Diketopyrrolopyrrole Moiety as a Promising Building Block to Enable Balanced Ambipolar Polymers for Flexible Transistors. *Adv. Mater.* **2017**, *29*, 1606162.
- (14) Cheng, Y. J.; Yang, S. H.; Hsu, C. S. Synthesis of Conjugated Polymers for Organic Solar Cell Applications. *Chem. Rev.* **2009**, *109*, 5868–5923.
- (15) Chen, H.; Wadsworth, A.; Ma, C.; Nanni, A.; Zhang, W.; Nikolka, M.; Luci, A. M. T.; Perdigão, L. M. A.; Thorley, K. J.; Cendra, C.; Larson, B.; Rumbles, G.; Anthopoulos, T. D.; Salleo, A.; Costantini, G.; Sirringhaus, H.; McCulloch, I. The Effect of Ring Expansion in Thienobenzob[*b*]Indacenodithiophene Polymers for Organic Field-Effect Transistors. *J. Am. Chem. Soc.* **2019**, *141*, 18806–18813.
- (16) Wadsworth, A.; Chen, H.; Thorley, K. J.; Cendra, C.; Nikolka, M.; Bristow, H.; Moser, M.; Salleo, A.; Anthopoulos, T. D.; Sirringhaus, H.; McCulloch, I. Modification of Indacenodithiophene-Based Polymers and Its Impact on Charge Carrier Mobility in Organic Thin-Film Transistors. *J. Am. Chem. Soc.* **2020**, *142*, 652–664.
- (17) Dou, J.; Chen, Z.; Ma, C. Regioregularity and Properties of the Poly(3-Hexylthiophene) Synthesized by Palladium Catalyzed Direct CH Arylation Polycondensation under Different Reaction Conditions. *Synth. Met.* **2014**, *196*, 117–124.
- (18) Allard, S.; Forster, M.; Souharce, B.; Thiem, H.; Scherf, U. Organic Semiconductors for Solution-Processable Field-Effect Transistors (OFETs). *Angew. Chem., Int. Ed.* **2008**, *47*, 4070–4098.
- (19) Aiyar, A. R.; Hong, J. I.; Reichmanis, E. Regioregularity and Intrachain Ordering: Impact on the Nanostructure and Charge Transport in Two-Dimensional Assemblies of Poly(3-Hexylthiophene). *Chem. Mater.* **2012**, *24*, 2845–2853.
- (20) Mei, J.; Bao, Z. Side Chain Engineering in Solution-Processable Conjugated Polymers. *Chem. Mater.* **2014**, *26*, 604–615.
- (21) Yaghoobi Nia, N.; Bonomo, M.; Zendehele, M.; Lamanna, E.; Desoky, M. M. H.; Paci, B.; Zurlo, F.; Generosi, A.; Barolo, C.; Viscardi, G.; Quagliotto, P.; Di Carlo, A. Impact of P3HT Regioregularity and Molecular Weight on the Efficiency and Stability of Perovskite Solar Cells. *ACS Sustainable Chem. Eng.* **2021**, *9*, 5061–5073.
- (22) Kline, R. J.; DeLongchamp, D. M.; Fischer, D. A.; Lin, E. K.; Richter, L. J.; Chabinyc, M. L.; Toney, M. F.; Heeney, M.; McCulloch, I. Critical Role of Side-Chain Attachment Density on the Order and Device Performance of Polythiophenes. *Macromolecules* **2007**, *40*, 7960–7965.
- (23) Ansari, M. A.; Mohiuddin, S.; Kandemirli, F.; Malik, M. I. Synthesis and Characterization of Poly(3-Hexylthiophene): Improvement of Regioregularity and Energy Band Gap. *RSC Adv.* **2018**, *8*, 8319–8328.
- (24) Lee, S.; Moon, G. D.; Jeong, U. Continuous Production of Uniform Poly(3-Hexylthiophene) (P3HT) Nanofibers by Electrospinning and Their Electrical Properties. *J. Mater. Chem.* **2009**, *19*, 743–748.
- (25) Na, J. Y.; Kang, B.; Park, Y. D. Influence of Molecular Weight on the Sulfidation of a Semiconducting Polymer during Time-Controlled Spin-Coating. *J. Phys. Chem. C* **2019**, *123*, 17102–17111.
- (26) Spangler, L. L.; Torkelson, J. M.; Royal, J. S. Influence of Solvent and Molecular Weight on Thickness and Surface Topography of Spin-coated Polymer Films. *Polym. Eng. Sci.* **1990**, *30*, 644–653.
- (27) Hong, S.; Lee, J.; Kang, H.; Lee, K. Slot-Die Coating Parameters of the Low-Viscosity Bulk-Heterojunction Materials Used for Polymer Solarcells. *Sol. Energy Mater. Sol. Cells* **2013**, *112*, 27–35.
- (28) Guilbert, A. A. Y.; Zbiri, M.; Dunbar, A. D. F.; Nelson, J. Quantitative Analysis of the Molecular Dynamics of P3HT:PCBM Bulk Heterojunction. *J. Phys. Chem. B* **2017**, *121*, 9073–9080.
- (29) McMahon, D. P.; Cheung, D. L.; Troisi, A. Why Holes and Electrons Separate so Well in Polymer/Fullerene Photovoltaic Cells. *J. Phys. Chem. Lett.* **2011**, *2*, 2737–2741.
- (30) Becker, O.; Sopade, P.; Bourdonnay, R.; Halley, P. J.; Simon, G. P. Layered Silicate Nanocomposites Based on Various High-Functionality Epoxy Resins. Part II: The Influence of an Organoclay on the Rheological Behavior of Epoxy Prepolymers. *Polym. Eng. Sci.* **2003**, *43*, 1683–1690.
- (31) Ito, S.; Fukuyama, M.; Tanaka, K.; Chujo, Y. Effects of Regioregularity of π -Conjugated Polymers Composed of Boron β -Diketiminato on Their Stimuli-Responsive Luminescence. *Macromol. Chem. Phys.* **2022**, *223*, 2100504.
- (32) Tremel, K.; Ludwigs, S. Morphology of P3HT in Thin Films in Relation to Optical and Electrical Properties. *Adv. Polym. Sci.* **2014**, *265*, 39–82.

- (33) Alberga, D.; Perrier, A.; Ciofini, I.; Mangiatordi, G. F.; Lattanzi, G.; Adamo, C. Morphological and Charge Transport Properties of Amorphous and Crystalline P3HT and PBTTT: Insights from Theory. *Phys. Chem. Chem. Phys.* **2015**, *17*, 18742–18750.
- (34) Tsoi, W. C.; James, D. T.; Kim, J. S.; Nicholson, P. G.; Murphy, C. E.; Bradley, D. D. C.; Nelson, J.; Kim, J. S. The Nature of In-Plane Skeleton Raman Modes of P3HT and Their Correlation to the Degree of Molecular Order in P3HT:PCBM Blend Thin Films. *J. Am. Chem. Soc.* **2011**, *133*, 9834–9843.
- (35) Poelking, C.; Andrienko, D. Effect of Polymorphism, Regioregularity and Paracrystallinity on Charge Transport in Poly(3-Hexylthiophene) [P3HT] Nanofibers. *Macromolecules* **2013**, *46*, 8941–8956.
- (36) Mauer, R.; Kastler, M.; Laquai, F. The Impact of Polymer Regioregularity on Charge Transport and Efficiency of P3HT:PCBM Photovoltaic Devices. *Adv. Funct. Mater.* **2010**, *20*, 2085–2092.
- (37) Kang, Y.; Kwak, D. H.; Kwon, J. E.; Kim, B. G.; Lee, W. H. NO₂-Affinitive Conjugated Polymer for Selective Sub-Parts-Per-Billion NO₂ Detection in a Field-Effect Transistor Sensor. *ACS Appl. Mater. Interfaces* **2021**, *13*, 31910–31918.
- (38) Choi, G.; Lee, K.; Oh, S.; Seo, J.; Park, E.; Park, Y. D.; Lee, J.; Lee, H. S. Electron-Interfered Field-Effect Transistors as a Sensing Platform for Detecting a Delicate Surface Chemical Reaction. *J. Mater. Chem. C* **2021**, *9*, 8179–8188.
- (39) Wei, S.; Tian, F.; Ge, F.; Wang, X.; Zhang, G.; Lu, H.; Yin, J.; Wu, Z.; Qiu, L. Helical Nanofibrils of Block Copolymer for High-Performance Ammonia Sensors. *ACS Appl. Mater. Interfaces* **2018**, *10*, 22504–22512.
- (40) Tang, X.; Girma, H. G.; Li, Z.; Hong, J.; Lim, B.; Jung, S. H.; Kim, Y.; Nam, S. Y.; Kim, K.; Kong, H.; Kim, S. H. “Dragging Mode” Electrohydrodynamic Jet Printing of Polymer-Wrapped Semiconducting Single-Walled Carbon Nanotubes for NO Gas-Sensing Field-Effect Transistors. *J. Mater. Chem. C* **2021**, *9*, 15804–15812.
- (41) Jordan, S. S.; Koros, W. J. A Free Volume Distribution Model of Gas Sorption and Dilation in Glassy Polymers. *Macromolecules* **1995**, *28*, 2228–2235.
- (42) Dissanayake, D. S.; Sheina, E.; Biewer, M. C.; McCullough, R. D.; Stefan, M. C. Determination of Absolute Molecular Weight of Regioregular Poly(3-Hexylthiophene) By ¹H-NMR Analysis. *J. Polym. Sci., Part A: Polym. Chem.* **2017**, *55*, 79–82.
- (43) Chan, K. H. K.; Yamao, T.; Kotaki, M.; Hotta, S. Unique Structural Features and Electrical Properties of Electrospun Conjugated Polymer Poly(3-Hexylthiophene) (P3HT) Fibers. *Synth. Met.* **2010**, *160*, 2587–2595.
- (44) Trznadel, M.; Pron, A.; Zagorska, M.; Chrzaszcz, R.; Pielichowski, J. Effect of Molecular Weight on Spectroscopic and Spectroelectrochemical Properties of Regioregular Poly(3-Hexylthiophene). *Macromolecules* **1998**, *31*, 5051–5058.
- (45) Oosterbaan, W. D.; Vrindts, V.; Berson, S.; Guillerez, S.; Douhéret, O.; Ruttens, B.; D’Haen, J.; Adriaenssens, P.; Manca, J.; Lutsen, L.; Vanderzande, D. Efficient Formation, Isolation and Characterization of Poly(3-Alkylthiophene) Nanofibres: Probing Order as a Function of Side-Chain Length. *J. Mater. Chem.* **2009**, *19*, 5424–5435.
- (46) Goh, R. G. S.; Waclawik, E. R.; Motta, N.; Bell, J. M. Influence of Dispersed Carbon Nanotubes on the Optical and Structural Properties of a Conjugated Polymer. *Device Process Technologies for Microelectronics MEMS, Photonics IV*; SPIE, 2006; Vol. 6037, p 264.
- (47) Kline, R. J.; McGehee, M. D.; Kadnikova, E. N.; Liu, J.; Fréchet, J. M. J.; Toney, M. F. Dependence of Regioregular Poly(3-Hexylthiophene) Film Morphology and Field-Effect Mobility on Molecular Weight. *Macromolecules* **2005**, *38*, 3312–3319.
- (48) Jang, D.; Park, Y. D. Addition of En-APTAS to a Polythiophene Film for Enhanced NO₂ Gas Sensing. *ACS Appl. Electron. Mater.* **2022**, *4*, 6300–6307.
- (49) Kwon, E. H.; An, H.; Park, M. B.; Kim, M.; Park, Y. D. Conjugated Polymer–Zeolite Hybrids for Robust Gas Sensors: Effect of Zeolite Surface Area on NO₂ Sensing Ability. *Chem. Eng. J.* **2021**, *420*, 129588.
- (50) Gao, C. Y.; Pei, M.; Choi, H. J.; Yang, H. Spontaneous Phase Separation of Poly(3-Hexylthiophene)s with Different Regioregularity for a Stretchable Semiconducting Film. *Adv. Funct. Mater.* **2019**, *29*, 1903163.